Ion and electron heating at quasi-parallel bow shocks

Krzysztof Stasiewicz[1]

[1]University of Zielona Góra

November 26, 2022

Abstract

Measurements from the Magnetospheric Multiscale (MMS) mission indicate that the density gradients associated with nonlinear compressional structures (shocklets) in a quasi-parallel bow shock trigger sequentially two instabilities that heat ions and electrons. The Lower-Hybrid-Drift (LHD) instability, triggered by the diamagnetic drift of ions, produces electric fields and ExB drift of electrons that triggers the Electron-Cyclotron-Drift (ECD) instability. Both instabilities create large amplitude electric fields $\sim$20–200 mV/m at wavelengths comparable to the electron gyroradius. Strong gradients of the electric field lead to stochastic heating of both ions and electrons, controlled by a dimensionless function $\chi = m_iq_i^{-1} B^{-2}\mathrm{div}(\mathbf{E}_\perp)$, which represents a universal, non-resonant heating mechanism for particles species with mass m_i and charge q_i, independent of the type of waves and instabilities.

Ion and electron heating at quasi-parallel bow shocks

Krzysztof Stasiewicz

[1]Department of Physics and Astronomy, University of Zielona Góra, Poland
[2]Space Research Centre, Polish Academy of Sciences, Warsaw, Poland

Key Points:

- Density gradients of nonlinear compressional structures (shocklets) in quasi-parallel shocks trigger the Lower-Hybrid-Drift (LHD) instability.
- The LHD instability creates fast ExB drifts of electrons, which trigger the Electron-Cyclotron-Drift (ECD) instability.
- Both LHD and ECD instabilities create large amplitude electric fields, which via a stochastic mechanism lead to ion and electron heating at shock waves.

Corresponding author: Krzysztof Stasiewicz, krzy.stasiewicz@gmail.com

Abstract

Measurements from the Magnetospheric Multiscale (MMS) mission indicate that the density gradients associated with nonlinear compressional structures (shocklets) in a quasi-parallel bow shock trigger sequentially two instabilities that heat ions and electrons. The Lower-Hybrid-Drift (LHD) instability, triggered by the diamagnetic drift of ions, produces electric fields and ExB drift of electrons that triggers the Electron-Cyclotron-Drift (ECD) instability. Both instabilities create large amplitude electric fields ∼20–200 mV/m at wavelengths comparable to the electron gyroradius. Strong gradients of the electric field lead to stochastic heating of both ions and electrons, controlled by a dimensionless function $\chi = m_i q_i^{-1} B^{-2} \mathrm{div}(\mathbf{E}_\perp)$, which represents a universal, non-resonant heating mechanism for particles species with mass m_i and charge q_i, independent of the type of waves and instabilities.

Plain Language Summary

Collisionless shocks in space represent amazing natural phenomena associated with a number of physical problems that attract a great deal of attention: turbulence, stochasticity, wave-particle interactions, nonlinear structures, shocklets, particle heating and acceleration. In astrophysics, shock acceleration is considered to be the primary acceleration mechanism. Using measurements from the Magnetospheric Multiscale (MMS) mission we demonstrate that ion and electron heating at the bow shock is caused by a stochastic mechanism related to gradients of the electric fields produced by the Lower-Hybrid-Drift (LHD) instability and the Electron-Cyclotron-Drift (ECD) instability.

1 Introduction

Collisionless shocks in space represent amazing natural phenomena associated with a number of physical problems that attract a great deal of attention: turbulence, stochasticity, wave-particle interactions, nonlinear structures, shocklets, particle heating and acceleration. In astrophysics, shock acceleration is considered to be the primary acceleration mechanism. Wherever energetic particles are produced, shocks are either observed to occur or are expected to do so, e.g., solar flares, corotating interaction regions in the solar wind, supernovae remnants, and accreting binary systems.

The most investigated plasma shock wave is the terrestrial bow shock formed at a distance of 14 R_E in front of the Earth, where the solar wind collides with the outermost regions of the magnetosphere. It is well known that shocks thermalise incoming solar wind, and produce also some energetic particles. There are a variety of processes that can heat and energise particles in a collisionless plasma. In reviews by Wu et al. (1984); Gary (1993); Treumann (2009); Burgess et al. (2012) one can find a long list of instabilities that could play a role in ion and electron heating – however, insufficient support from observations put the question on the dominant mechanism into inconclusive state.

On the basis of measurements from the Magnetospheric Multiscale MMS mission (Burch et al., 2016), it has been shown (Stasiewicz, 2020) that particle heating at quasi-perpendicular bow shocks is related to two drift instabilities: the Lower-Hybrid-Drift, and the Electron-Cyclotron-Drift instability. The LHD instability is a cross-field current-driven instability generated on the density gradients, when the diamagnetic drift of ions (assumed protons) $V_d = T_p(m_p\omega_{cp}L_n)^{-1} = v_{tp}(r_p/L_n)$ is comparable to the thermal ion speed, $v_{tp} = (T_p/m_p)^{1/2}$, or equivalently when the scale of the density gradient $L_n = (N^{-1}|\nabla N|)^{-1}$ is comparable to the ion cyclotron radius $r_p = v_{tp}/\omega_{cp}$. Here, T_p, m_p, ω_{cp} are proton temperature, mass, and cyclotron frequency. The maximum growth rate is at $k_\perp r_e \sim 1$, i.e., at wavelengths of a few electron gyroradii (Davidson et al., 1977; Huba et al., 1978; Daughton, 2003).

The LHD instability creates electric fields, which lead to strong ExB drifts of electrons only, because ions are not subject to this drift due to the large gyroradius in comparison to the width of drift channels, and also due to frequency much greater than the ion gyrofrequency. When the electron drift speed becomes comparable to the thermal speed, $V_E \sim v_{te}$, the ECD instability is initiated, which produces shorter wavelengths and occurs at the resonance $k_\perp V_E \sim n\omega_{ce}$ that couples electron Bernstein modes with ion-acoustic waves (Forslund et al., 1972; Lashmore-Davies, 1971; Muschietti & Lembége, 2013). The ECD waves have been identified at the bow shock in measurements from STEREO, Wind and MMS (Wilson III et al., 2010; Breneman et al., 2013; Goodrich et al., 2018). It is interesting to note that the same ExB drift of electrons excites the ECD instability in space and in Hall ion thrusters (Boeuf & Garrigues, 2018).

These two instabilities generate large amplitude electric fields 20–200 mV/m on short spatial scales ($\sim r_e$) that perturb orbits of gyrating ions and electrons by breaking the magnetic moments and causing chaotic particle movements. This facilitates efficient stochastic heating by the present electric fluctuations, and even by the DC field. The condition for stochastic heating of particles with mass m_i, charge q_i is (Stasiewicz, 2020)

$$\chi_i(t, \mathbf{r}) = \frac{m_i}{q_i B^2}\mathrm{div}(\mathbf{E}_\perp); \ |\chi_i| > 1. \tag{1}$$

This condition with divergence reduced to the directional gradient $\partial_x E_x$, has been used by several authors to explain heating of particles in laboratory and space (Cole, 1976; McChesney et al., 1987; Karney, 1979; Balikhin et al., 1993; Gedalin et al., 1995; Mishin & Banaszkiewicz, 1998; Stasiewicz et al., 2000; Stasiewicz, 2007; Vranjes & Poedts, 2010; Stasiewicz et al., 2013; See et al., 2013; Yoon & Bellan, 2019). The heating function can be regarded as a quantitative measure of the demagnetisation of the particle species m_i. It is also related to the charge non-neutrality, because $\chi = (N_c/N)(c^2/V_{Ai}^2)$, where $V_{Ai}^2 = B^2/(\mu_0 N m_i)$, upon substitution $\mathrm{div}(\mathbf{E}) = N_c q_i/\epsilon_0$. However, only $\mathbf{E}_\perp$ is put into (1) to exclude modes with $E_\parallel$, like Langmuir or ion acoustic waves that do not contribute to the stochasticity.

The scenario outlined above has been deduced from the analysis of MMS measurements at a quasi-perpendicular shock, so it would be interesting to check whether it is applicable also for quasi-parallel shocks, which is the purpose of this Letter.

2 Observations

We use here plasma parameters provided by the Fast Plasma Investigation (Pollock et al., 2016) on MMS, measurements of the electric field (Lindqvist et al., 2016; Ergun et al., 2016; Torbert et al., 2016) and the magnetic field measured by the Fluxgate Magnetometer (Russell et al., 2016).

When the interplanetary magnetic field is in the direction quasi-parallel to the shock normal, instead of a single ramp of the perpendicular bow shock, an extended foreshock region is formed, filled with nonlinear compressional structures (shocklets) similar to those shown in Fig. 1a. These shocklets have spatial scales of ∼1,000 km and represent compressions of the plasma density and the magnetic field by a factor 2–10 times the background values (Schwartz & Burgess, 1991; Stasiewicz et al., 2003; Lucek et al., 2008; Wilson III et al., 2013). The large amplitude shocklets are standing against the solar wind flow and move with respect to spacecraft with speed of $\sim$ 10 km/s. In the vicinity of the shocklets in Fig. 1a we observe intense electron heating shown in panel 1b (increase of T_e by a factor of 4), and the ion heating shown in panel 1c (increase of $T_i = T_p$ by a factor of 8).

Figure 1a indicates presence of strong gradients of the density, so we expect that the region may be unstable for the LHD instability. To verify that this is the case we compute the gradient scale $L_N = (N^{-1}|\nabla N|)^{-1}$ for the plasma density using a gen-

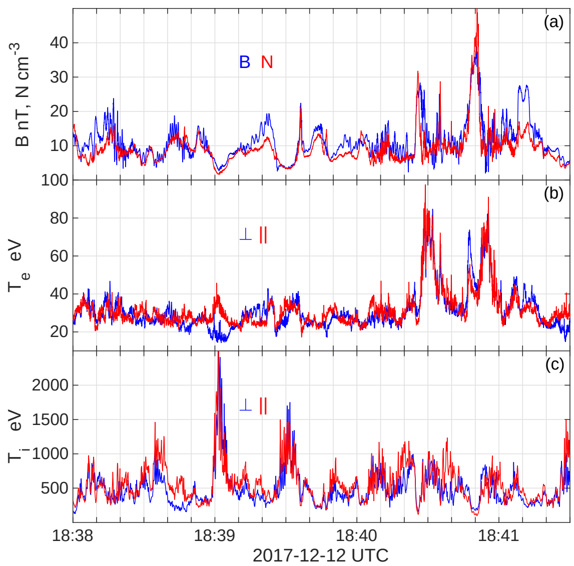

Figure 1. MMS-1 measurements from a 3.5 min time interval of a quasi-parallel bow shock: (a) magnetic field B, and electron number density N that form large amplitude compressional structures (shocklets) – typical for parallel shocks. Perpendicular and parallel temperatures of electrons (b), and ions (c) exhibit spectacular heating events.

eral method for computing gradients from 4–point measurements developed for Cluster (Harvey, 1998). The same method is applied to compute div($\mathbf{E}_\perp$), used in the function χ. This function is computed with the electric field in the frequency range 0.15–4096 Hz. The lowest frequencies were removed to avoid DC calibration offsets and possible effects of the satellite spin period (f=0.05 Hz, and harmonics). The mean characteristic frequencies in this interval are: the proton cyclotron f_{cp}=0.2 Hz, the lower hybrid f_{lh}=7 Hz, the electron cyclotron f_{ce}=300 Hz, and the proton plasma f_{pp}=620 Hz.

The result of L_N determination is shown in Fig.2a. In most of the region, $L_N/r_p < 1$, indicating that the region is strongly unstable for the LHD instability.

In the next step, we compute $V_E = \mathbf{E} \times \mathbf{B}/B^2$ to check if electrons are prone to the ECD instability. The result in panel 2b shows that in a significant part of the region we have condition $V_E > v_{te}$, that would produce strong ECD instability. The ExB drift is computed with the full spectrum of the measured electric field, including frequencies $> f_{ce}$, which would invalidate the drift approximation. Therefore it should not be assumed that bulk electrons attain everywhere the computed values of V_E.

The electric fields developed by LHD and ECD instabilities (maximum = 220 mV/m) produce stochastic heating function χ shown in panel 2c that has maximum value $\chi = \chi_p$=11,355, computed with the proton mass. This is equivalent to the electron χ_e=6.1, indicating favourable conditions for strong stochastic heating of electrons, which is indeed observed in Fig. 1b. Because the separation of the MMS constellation is about 15 km, we cannot properly compute gradients on scales less than 10 km, which means that the computed values of χ may underestimate the real ones, because the ECD waves are expected to have wavelengths on the order of the electron cyclotron radius ∼1 km (Muschietti & Lembége, 2013). Other errors in derivation of χ are the same as in measurements of the electric field, i.e. ca 10% (Torbert et al., 2016).

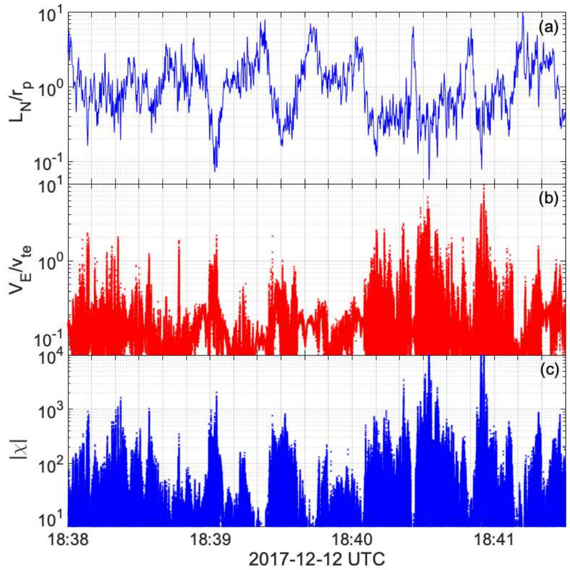

Figure 2. Diagnostic parameters for the case of Fig. 1: (a) The gradient scale of the plasma density L_N is normalised with thermal ion gyroradius r_p (mean = 250 km). $L_N/r_p < 1$ implies that the region is strongly unstable for the LHD instability. (b) The computed ExB drift normalised with the electron thermal speed v_{te} (mean = 2300 km/s). $V_E/v_{te} > 1$ implies that the region is strongly unstable for the ECD instability. (c) Function χ (maximum = 11,355) derived from the data with equation (1) for the electric field 0.15–4096 Hz, and the proton mass, m_p.

Minima of L_N in Figure 2a correspond to the maxima of V_E in panel 2b, and also with maxima of the heating function in panel 2c. This indicates that the heating of both ions and electrons is initiated by the LHD instability on density gradients that evolves in place into the ECD instability created by V_E drifts, as seen in panel 2b. It is also seen that the regions with $L_N/r_p > 4$ have reduced V_E in panel 2b (weak electric field), and small values of the heating function in panel 2c. This means that the observed onset of the LHD instability is surprisingly close to the theoretical threshold, $L_N/r_p < (m_p/m_e)^{1/4} \approx 6$, derived some 40 years ago (Huba et al., 1978).

Generally, all diagnostic parameters shown in Figure 2 are consistent with the heating observed in Figure 1, and also with the scenario described in the Introduction. The highest temperatures of electrons in Fig. 1b correspond to χ_e=6.1 in Fig. 2c, which clearly associates electron heating with function χ.

In the following we shall investigate in detail properties of waves responsible for electron and ion heating observed in Fig. 1.

2.1 Electron heating and ECD waves

In Figure 3 we show some details of the electron heating event from Fig. 1b. The maximum of the electron temperature corresponds to χ_e =6.1. Such a large value for the heating function is related to the local minimum of B. Heating of both electrons and ions (see also Fig. 6) occur preferentially in the local minima of B, consistent with χ as the controlling function, because of dependence $\chi \propto B^{-2}$. Quenching of the heating at B >20 nT is also consistent with this mechanism.

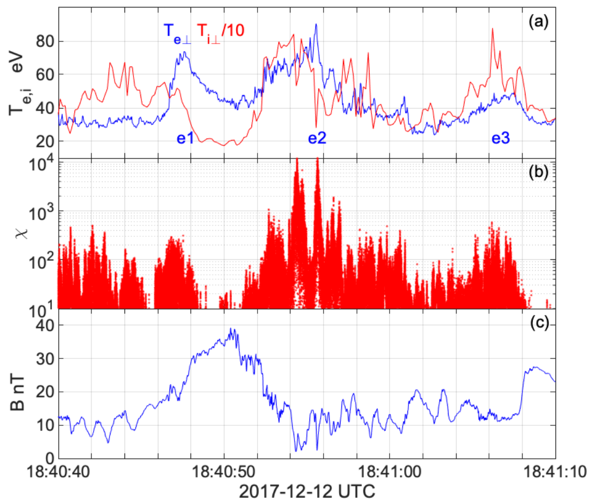

Figure 3. Zoom (30 s) of the electron heating event from Fig. 1: (a) Electron and ion temperatures ($T_{i\perp}/10$), (b) χ function, (c) magnetic field B.

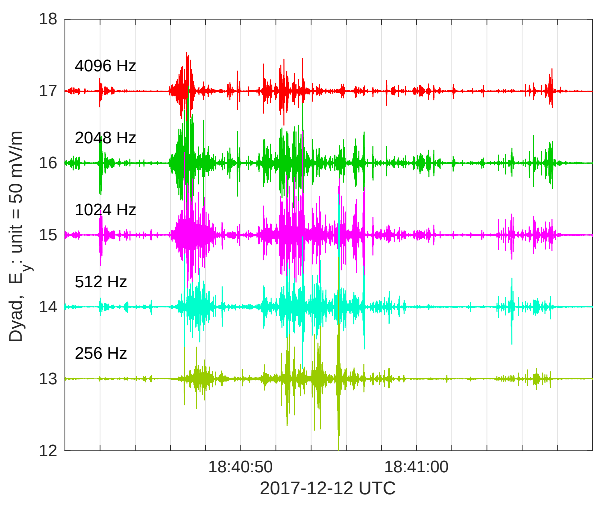

Figure 4. Waves measured by MMS-1 in the region of Fig. 3. The electric field perpendicular component $E_{y\perp}$ is decomposed in discrete frequency dyads in the range 256–4096 Hz that correspond to the Electron-Cyclotron-Drift waves.

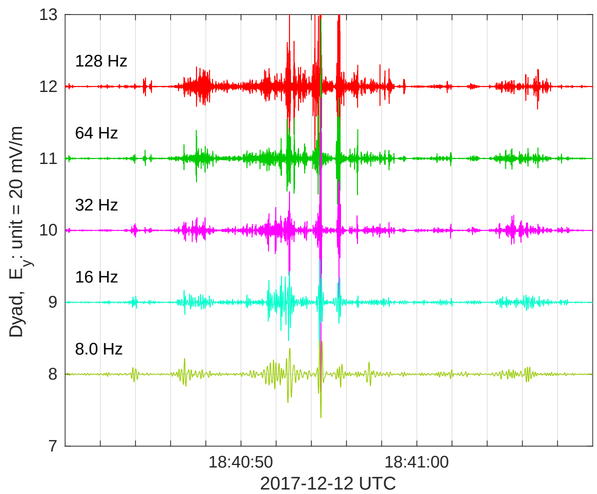

Figure 5. Continuation of Fig. 4 to lower frequencies that cover Lower-Hybrid-Drift waves, 8–128 Hz.

Figure 4 shows the measured signal $E_{y\perp}$ decomposed into discrete frequency dyads with orthogonal wavelets (Mallat, 1999). Orthogonality means that the time integral of the product of any pair of the frequency dyads is zero, and the decomposition is exact, i.e., the sum of all components gives the original signal. This frequency range corresponds to the Electron-Cyclotron-Drift waves that start around f_{ce} ~300 Hz and extend to the upper frequency of the measurements. The border frequencies should not be regarded as strict, because Doppler shifts of short wavelengths would produce considerable spread and overlap of modes. The labels on the y-axis represent dyad numbers, and the unit range corresponds to the amplitude 50 mV/m. Waves in this frequency range have been analyzed with use of high-time resolution measurements obtained by THEMIS (Mozer & Sundqvist, 2013; Wilson III et al., 2014), who noted large parallel electric field components in these modes and attributed it to ion acoustic waves. The presence of electron cyclotron harmonics in the spectra has led to their identification as ECD waves (Wilson III et al., 2010; Breneman et al., 2013; Goodrich et al., 2018; Stasiewicz, 2020).

2.2 Ion heating and LHD waves

Figure 5 is the extension of Fig. 4 to lower frequencies covered by Lower-Hybrid-Drift waves that start from $f_{lh} \sim 7$ Hz and extend to f_{ce}. They exhibit perpendicular direction for the Poynting flux and rapidly diminishing magnetic component with increasing frequency. Obliquely propagating whistler and/or magnetosonic waves are also observed in this region at frequencies below f_{lh}. LH and LHD waves have been observed also in other regions of the magnetosphere (Bale et al., 2002; Vaivads et al., 2004; Norgren et al., 2012; Graham et al., 2017).

The LHD waves in Fig. 5 maximise at the minima of L_N, i.e., at the maxima of the density gradients, and have theoretical maximum growth rate at $k_\perp r_e$ ~1. The electric field of these waves generates ExB drift of electrons that ignites the ECD instability via the resonance $k_\perp V_E \sim n\omega_{ce}$. This resonance condition can be expressed equivalently by $k_\perp r_e \sim n v_{te}/V_E$, which means that the ECD waves resonate/couple with structures created by the LHD instability, $k_\perp r_e \sim 1$ when $n v_{te}/V_E = 1$. There is smooth transition and co-location of LHD, and ECD waves, seen in Figures 4,5 which is possibly related to the matching condition between these two instabilities. The n=1 ECD mode

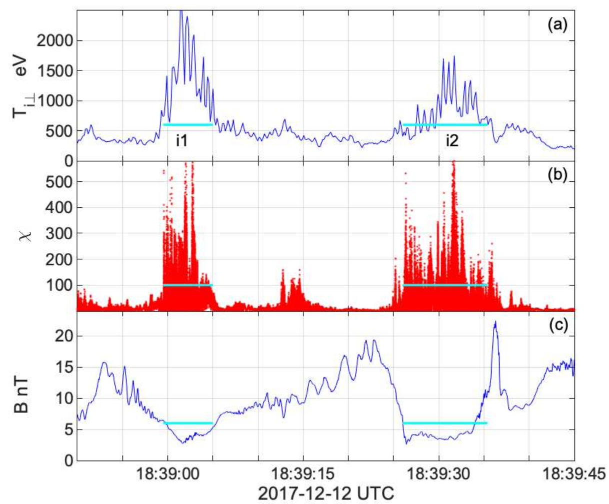

Figure 6. Zoom at the ion heating event from Fig. 1: (a) Ion temperature, (b) χ function, (c) magnetic field B. Note that heating occurs preferentially in depressions of B, consistent with Equation (1).

can be naturally excited in drift channels created by the LHD instability when $V_E = v_{te}$.

In Figure 6 we concentrate on the ion heating event from Fig. 1c. The ion heating is remarkably strong in this event but the amplitude of LHD waves in this case is only ∼10 mV/m, significantly smaller than for waves shown in Fig. 5. The heating function is, however, quite large because B drops below 5 nT in this case. Ions perturbed stochastically by $\chi_p \gg 1$ can be energised either by fluctuating, wave fields, and/or by the DC field,

$$\Delta W = q_i \langle \mathbf{v} \cdot (\mathbf{E}_0 + \delta \mathbf{E}) \rangle. \tag{2}$$

The quasi-DC field (below $f_{cp} \approx 0.2$ Hz) in this region is $E_0 \sim 2.5$ mV/m, while the gyroradius is $r_p \sim 800$ km. On the distance of r_p we have potential of 2000 V, sufficient to explain the observed energisation of ions. The stochastic acceleration on fluctuating fields would represent a diffusive process, requiring longer times with statistically significant number of interactions, while the DC acceleration, or generally by the electric field of waves with frequencies lower than the gyrofrequency and wavelengths larger than the gyroradius, could be a rapid, single step event (Stasiewicz, 2007). In this model a cold particle is convected on a single $\partial_x E_x$ structure and acquires large gyroradius after encounter. The perpendicular energisation is done by the convection potential after stochastic demagnetisation by $\chi > 1$. Details of the heating process, the relative importance of the DC- and wave- acceleration, dependence on the ratio of scales of the structures/gyroradius, and the frequency of waves/gyrofrequency can be resolved by suitable simulations, which will be the subject of a separate publication.

3 Conclusions

The analysis of the MMS measurements leads to the following conclusions on the heating mechanism at quasi-parallel shock waves:

Large amplitude shocklets, i.e., compressions of N and B observed at quasi-parallel shocks are associated with density gradients on spatial scales exceeding the threshold for the onset of the Lower-Hybrid-Drift instability, $L_N < r_p$.

The LHD instability creates electric fields, $E \sim$20 mV/m in the frequency range $[f_{lh}, f_{ce}]$, that cause ExB drift of electrons in narrow channels, $k_\perp r_e \sim$1, with speed $V_E > v_{te}$, that leads to the Electron-Cyclotron-Drift instability.

The ECD instability creates larger electric fields, $E \sim$ 200 mV/m at frequencies $f \geq f_{ce}$, on wavelengths $\sim r_e$, and smaller, Doppler spread over wide frequency range.

Large gradients of the electric fields created by LHD and ECD instabilities produce conditions such that the heating functions (1) become $\chi_p \gg$1, and $\chi_e \gg$1, which leads to the stochastic heating of ions and electrons.

The non-adiabatic heating of ions and electrons occurs preferentially at the local minima of B, consistent with Equation (1).

Acknowledgments

The author thanks members of the MMS mission for making available the data and is grateful to Yuri Khotyaintsev for his invaluable help with the software for data processing. MMS science data is made available through the Science Data Center at the Laboratory for Atmospheric and Space Physics (LASP) at the University of Colorado, Boulder: https://lasp.colorado.edu/mms/sdc/public/.

References

Bale, S. D., Mozer, F. S., & Phan, T. (2002). Observation of lower hybrid drift instability in the diffusion region at a reconnecting magnetopause. *Geophys. Res. Lett.*, *29*, 33-1-33-4. doi: 10.1029/2002GL016113

Balikhin, M., Gedalin, M., & Petrukovich, A. (1993). New mechanism for electron heating in shocks. *Phys. Rev. Lett.*, *70*, 1259. doi: 10.1103/PhysRevLett.70.1259

Boeuf, J. P., & Garrigues, L. (2018). ExB electron drift instability in Hall thruster: particle-in-cell simulations vs theory. *Phys. Plasmas*, *25*, 061204. doi: 10.1063/1.5017033

Breneman, A. W., Cattell, C. A., Kersten, K., et al. (2013). Stereo and wind observations of intense cyclotron harmonic waves at the earth's bow shock and inside the magnetosheath. *J. Geophys. Res.*, *118*, 7654-7664. doi: 10.1002/2013JA019372

Burch, J. L., Moore, R. E., Torbert, R. B., & Giles, B. L. (2016). Magnetospheric multiscale overview and science objectives. *Space Sci. Rev.*, *199*(1), 1-17. doi: 10.1007/s11214-015-0164-9

Burgess, D., Möbius, E., & Scholer, M. (2012). Ion acceleration at the Earth's bow shock. *Space Sci. Rev.*, *173*, 5-47. doi: 10.1007/s11214-012-9901-5

Cole, K. D. (1976). Effects of crossed magnetic and spatially dependent electric fields on charged particle motion. *Planet. Space Sci.*, *24*, 515-518. doi: 10.1016/0032-0633(76)90096-9

Daughton, W. (2003). Electromagnetic properties of the lower- hybrid drift instability in a thin current sheet. *Phys. Plasmas*, *10*, 3103. doi: 10.1063/1.1594724

Davidson, R. C., Gladd, N. T., Wu, C., & Huba, J. D. (1977). Effects of finite plasma beta on the lower-hybrid-drift instability. *Phys. Fluids*, *20*, 301. doi: 10.1063/1.861867

Ergun, R. E., Tucker, S., Westfall, J., et al. (2016). The axial double probe and fields signal processing for the MMS mission. *Space Sci. Rev.*, *199*, 167-188. doi: 10.1007/s11214-014-0115-x

Forslund, D., Morse, R., Nielson, C., & Fu, J. (1972). Electron cyclotron drift instability and turbulence. *Phys. Fluids*, *15*, 1303. doi: 10.1063/1.1694082

Gary, S. P. (1993). *Theory of space plasma microinstabilities.* Cambridge University Press.

Gedalin, M., Gedalin, K., Balikhin, M., & Krasnosselskikh, V. (1995). Demagnetization of electrons in the electromagnetic field structure, typical for quasi-perpendicular collisionless shock front. *J. Geophys. Res.*, *100*, 9481-9488. doi: 10.1029/94JA03369

Goodrich, K. A., Ergun, R., Schwartz, S. J., Wilson III, L., Newman, D., Wilder, F. D., ... Andersson, L. (2018). Mms observations of electrostatic waves in an oblique shock crossing. *J. Geophys. Res.*, *123*(11), 9430-9442. doi: 10.1029/2018JA025830

Graham, D. B., Khotyaintsev, Y. V., Norgren, C., et al. (2017). Lower hybrid waves in the ion diffusion and magnetospheric inflow regions. *J. Geophys. Res.*, *122*, 517-533. doi: 10.1002/2016JA023572

Harvey, C. C. (1998). Spatial gradients and the volumetric tensor. In G. Paschmann & P. W. Daly (Eds.), *Analysis methods for multi-spacecraft data* (Vol. SR-001 ISSI Reports, p. 307-322). ESA.

Huba, J. D., Gladd, N. T., & Papadopoulos, K. (1978). Lower-hybrid-drift wave turbulence in the distant magnetotail. *J. Geophys. Res.*, *A11*, 5217. doi: 10.1029/JA083iA11p05217

Karney, C. F. F. (1979). Stochastic ion heating by a lower hybrid wave. *Phys. Fluids*, *22*, 2188. doi: 10.1063/1.862512

Lashmore-Davies, C. N. (1971). Instability in a perpendicular collisionless shock wave for arbitrary ion temperature. *Phys. Fluids*, *14*, 1481. doi: 10.1063/1.1693632

Lindqvist, P.-A., Olsson, G., Torbert, R. B., et al. (2016). The spin-plane double probe electric field instrument for MMS. *Space Sci. Rev.*, *199*, 137-165. doi: 10.1007/s11214-014-0116-9

Lucek, E. A., Horbury, T. S., Dandouras, I., & Reme, H. (2008). Cluster observations of the Earth's quasi-parallel bow shock. *JGR*, *113*, A07S02. doi: 10.1029/2007JA012756

Mallat, S. (1999). *A wavelet tour of signal processing.* Academic Press.

McChesney, J. M., Stern, R., & Bellan, P. M. (1987). Observation of fast stochastic ion heating by drift waves. *Phys. Rev. Lett.*, *59*, 1436. doi: 10.1103/PhysRevLett.59.1436

Mishin, E., & Banaszkiewicz, M. (1998). On auroral ion conics and electron beams acceleration. *Geophys. Res. Lett.*, *25*, 4309-4312. doi: 10.1029/1998GL900165

Mozer, F. S., & Sundqvist, D. (2013). Electron demagnetization and heating in quasi-perpendicular shocks. *J. Geophys. Res.*, *118*, 5415-5420. doi: 10.1002/jgra.50534

Muschietti, L., & Lembége, B. (2013). Microturbulence in the electron cyclotron frequency range at perpendicular supercritical shocks. *J. Geophys. Res.*, *118*(5), 2267-2285. doi: 10.1002/jgra.50224

Norgren, C., Vaivads, A., Khotyaintsev, Y., & André, M. (2012). Lower hybrid drift waves: space observations. *Phys. Rev. Lett.*, *109*, 055001. doi: 10.1103/PhysRevLett.109.055001

Pollock, C., Moore, T., Jacques, A., Burch, J., Gliese, U., Saito, Y., et al. (2016). Fast plasma investigation for magnetospheric multiscale. *Space Sci. Rev.*, *199*, 331-406. doi: 10.1007/s11214-016-0245-4

Russell, C. T., Anderson, B. J., Baumjohann, W., Bromund, K. R., Dearborn, D., Fischer, D., et al. (2016). The magnetospheric multiscale magnetometers. *Space Sci. Rev.*, *199*, 189-256. doi: 10.1007/s11214-014-0057-3

Schwartz, S. J., & Burgess, D. (1991). Quasi-parallel shocks: A patchwork of three-dimensional structures. *GeoRL*, *18*, 373. doi: 10.1029/91GL00138

See, V., Cameron, R. F., & Schwartz, S. J. (2013). Non-adiabatic electron behaviour due to short-scale electric field structures at collisionless shock waves. *Ann. Geophys.*, *31*, 639-646. doi: 10.5194/angeo-31-639-2013

Stasiewicz, K. (2007). Acceleration of particles in space plasmas by nonlinear magnetosonic waves. *Plasma Physics and Controlled Fusion*, *49*, B621–B628. doi: 10.1088/0741-3335/49/12b/s58

Stasiewicz, K. (2020). Stochastic ion and electron heating on drift instabilities at the bow shock. *MNRAS*, *496*, L133-L137. doi: 10.1093/mnrasl/slaa090

Stasiewicz, K., Longmore, M., Buchert, S., Shukla, P., Lavraud, B., & Picket, J. (2003). Properties of fast magnetosonic shocklets at the bow shock. *GeoRL*, *30*(24), 2241. doi: 10.1029/2003GL017971

Stasiewicz, K., Lundin, R., & Marklund, G. (2000). Stochastic ion heating by orbit chaotization on nonlinear waves and structures. *Physica Scripta*, *T84*, 60-63. doi: 10.1238/physica.topical.084a00060

Stasiewicz, K., Markidis, S., Eliasson, B., Strumik, M., & Yamauchi, M. (2013). Acceleration of solar wind ions to 1 MeV by electromagnetic structures upstream of the Earth's bow shock. *Europhys. Lett.*, *102*, 49001. doi: 10.1209/0295-5075/102/49001

Torbert, R. B., Russell, C. T., Magnes, W., Ergun, R. E., Lindqvist, P.-A., LeContel, O., et al. (2016). The FIELDS instrument suite on MMS. *Space Sci. Rev.*, *199*, 105-135. doi: 10.1007/s11214-014-0109-8

Treumann, R. A. (2009). Fundamentals of collisionless shocks for astro-physical application, 1. non-relativistic shocks. *Astron. Astrophys. Rev.*, *17*, 409-535. doi: 10.1007/s00159-009-0024-2

Vaivads, A., André, M., Buchert, S. C., Wahlund, J.-E., Fazakerly, A. N., & Cornileau-Wehrlin, N. (2004). Cluster observations of lower hybrid turbulence within thin layers at the magnetopause. *Geophys. Res. Lett.*, *31*, L03804. doi: 10.1029/2003GL018142

Vranjes, J., & Poedts, S. (2010). Drift waves in the corona: heating and acceleration of ions at frequencies far below the gyrofrequency. *MNRAS*, *408*, 1835–1839. doi: 10.1111/j.1365-2966.2010.17249.x

Wilson III, L. B., Cattell, C. A., Kellogg, P. J., Goetz, K., Kersten, K., Kasper, J. C., … Wilber, M. (2010). Large-amplitude electrostatic waves observed at a supercritical interplanetary shock. *J. Geophys. Res.*, *115*, A12104. doi: 10.1029/2010JA015332

Wilson III, L. B., Koval, A., Sibeck, D., Szabo, A., Cattell, C. A., Kasper, J. C., … Wilber, M. (2013). Shocklets, slams, and field-aligned ion beams in the terrestrial foreshock. *J. Geophys. Res.*, *118*, 953-966. doi: 10.1029/2012JA018186

Wilson III, L. B., Sibeck, D. G., Breneman, A. W., Le Contel, O., Cully, C., Turner, D. L., … Malaspina, D. M. (2014). Quantified energy dissipation rates in the terrestrial bow shock: 2. waves and dissipation. *J. Geophys. Res.*, *119*, 6475-6495. doi: 10.1002/2014JA019930

Wu, C. S., Winske, D., Zhou, Y. M., Tsai, S. T., Rodriguez, P., Tanaka, M., … Goodrich, C. C. (1984). Low-frequency instabilities in magnetic pulses. *Space Sci. Rev.*, *37*, 63-109. doi: 10.1007/BF00213958

Yoon, Y. D., & Bellan, P. M. (2019). Kinetic verification of the stochastic ion heating mechanism in collisionless magnetic reconnection. *ApJL*, *887*, L29. doi: 10.3847/2041-8213/ab5b0a

Figure1.

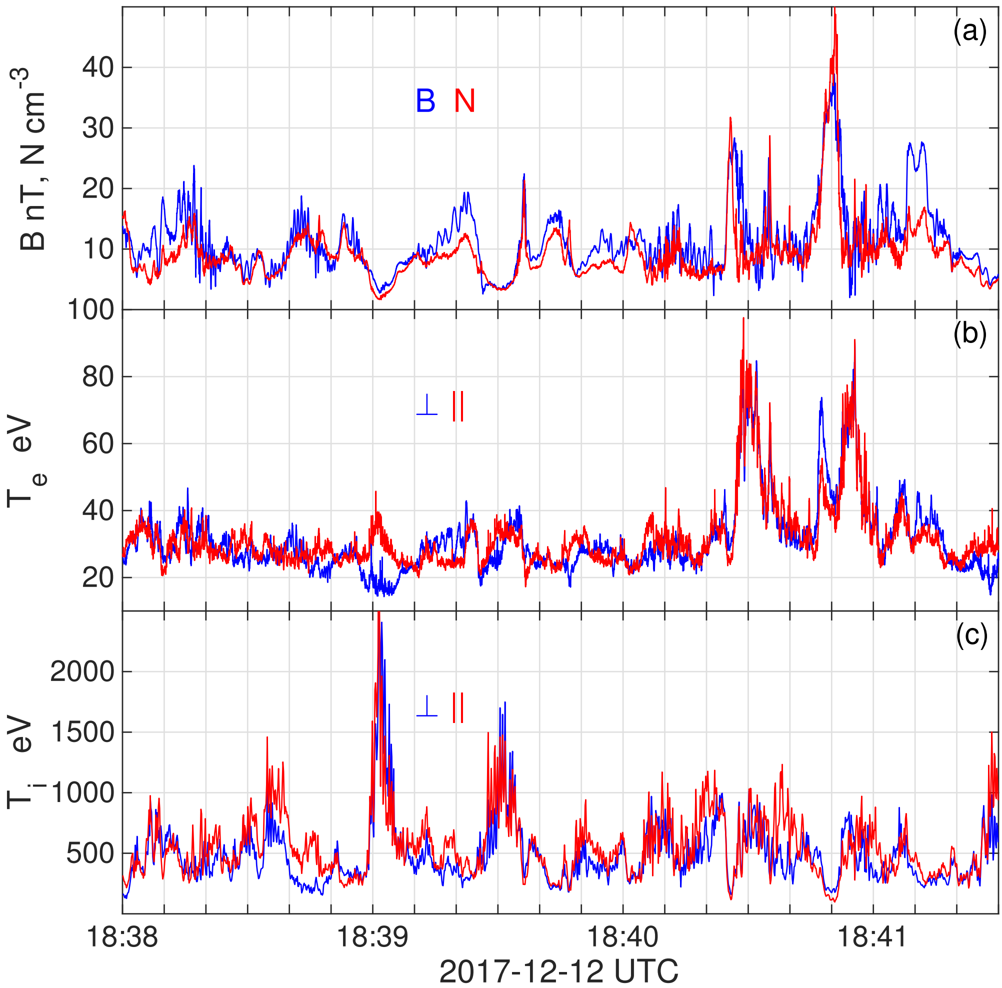

(a)
B N
B nT, N cm-3
(b)
⊥ ||
Te eV
(c)
⊥ ||
Ti eV
18:38
18:39
18:40
18:41
2017-12-12 UTC

Figure2.

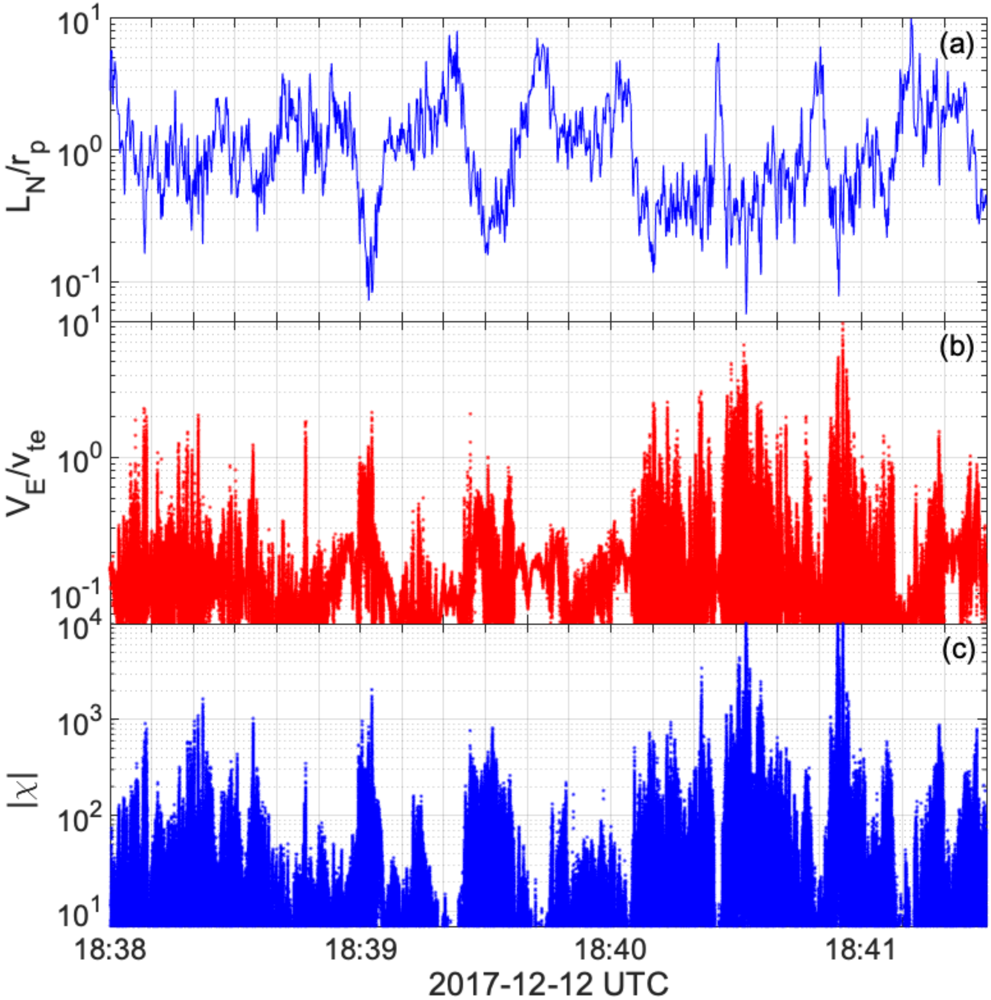

(a)
(b)
(c)
L_N/r_p
V_E/v_{te}
$|\chi|$
10^1
10^0
10^{-1}
10^4
10^3
10^2
18:38
18:39
18:40
18:41
2017-12-12 UTC

Figure3.

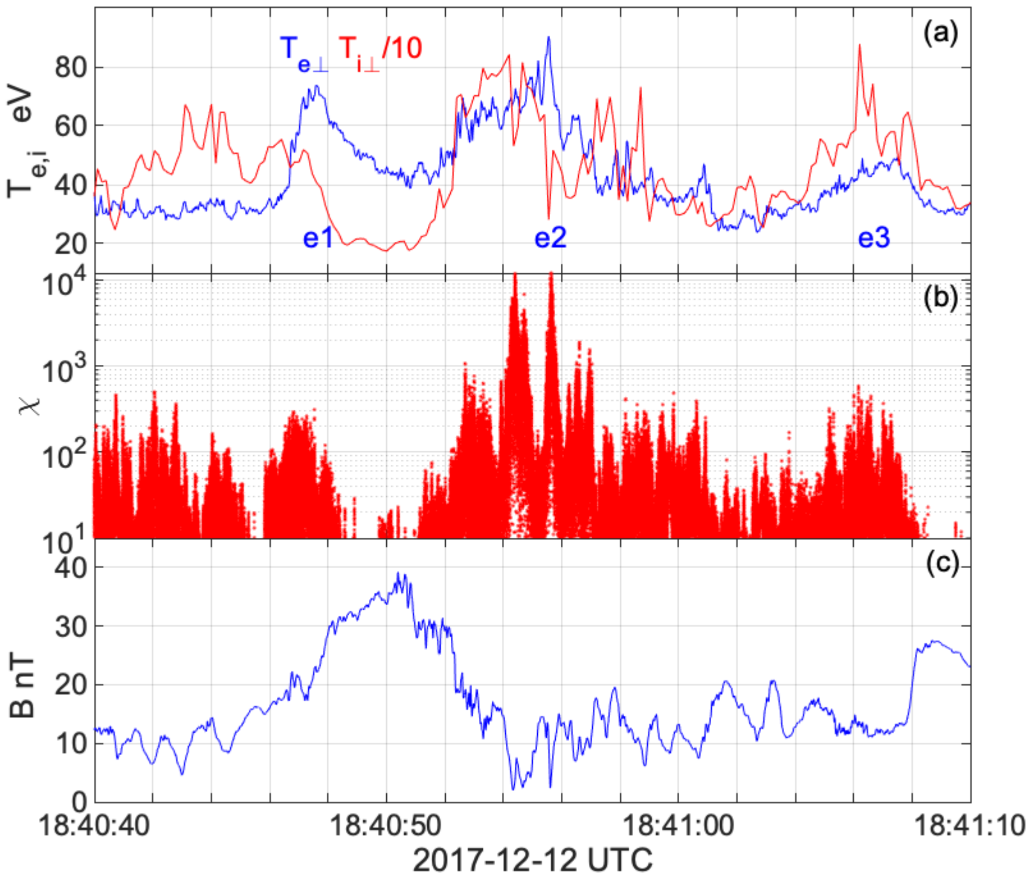

(a)
$T_{e\perp}$ $T_{i\perp}/10$
$T_{e,i}$ eV
e1
e2
e3
(b)
χ
(c)
B nT
18:40:40
18:40:50
18:41:00
18:41:10
2017-12-12 UTC

Figure4.

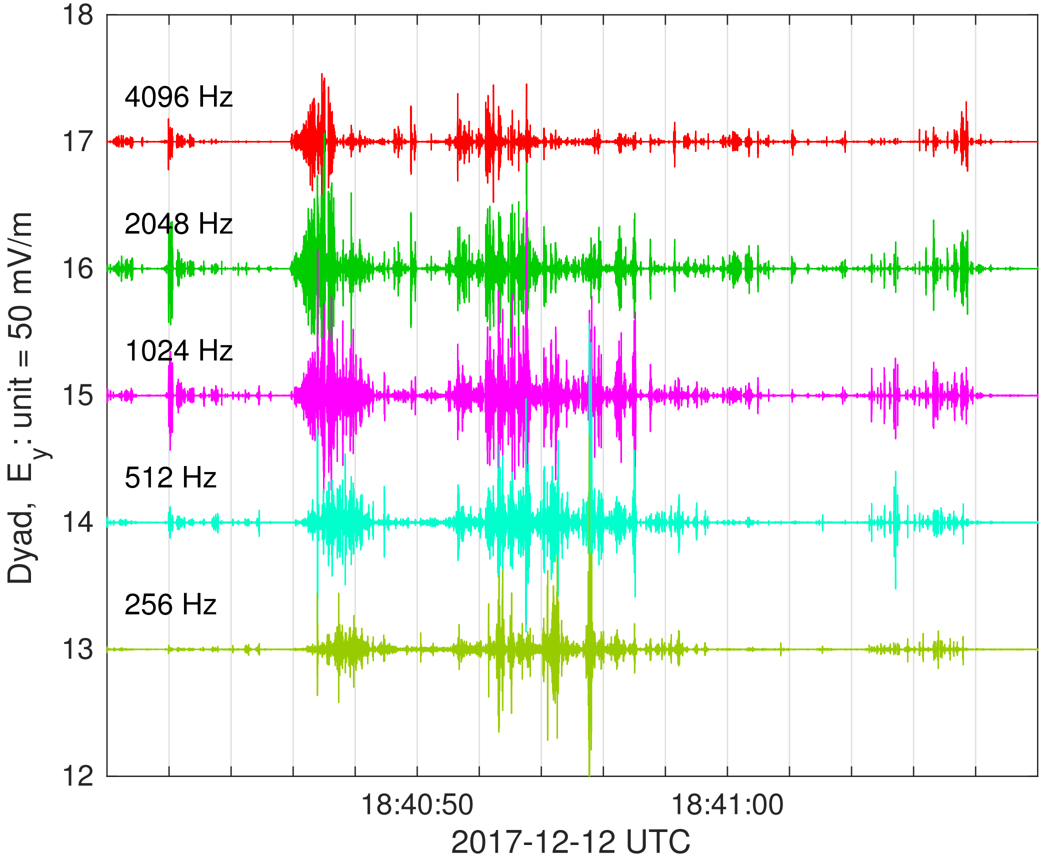
4096 Hz
2048 Hz
1024 Hz
512 Hz
256 Hz
18
17
16
15
14
13
12
Dyad, E_y: unit = 50 mV/m
18:40:50
18:41:00
2017-12-12 UTC

Figure5.

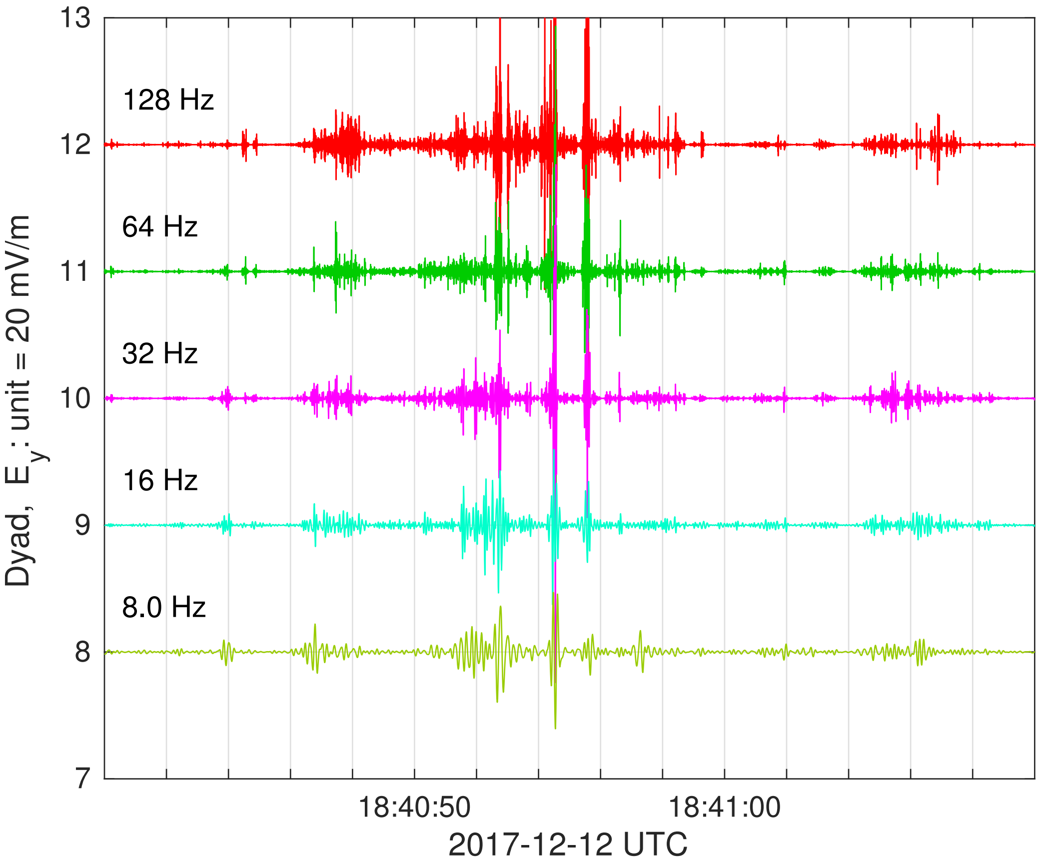

128 Hz
64 Hz
32 Hz
16 Hz
8.0 Hz
13
12
11
10
9
8
7
Dyad, E_y: unit = 20 mV/m
18:40:50
18:41:00
2017-12-12 UTC

Figure6.

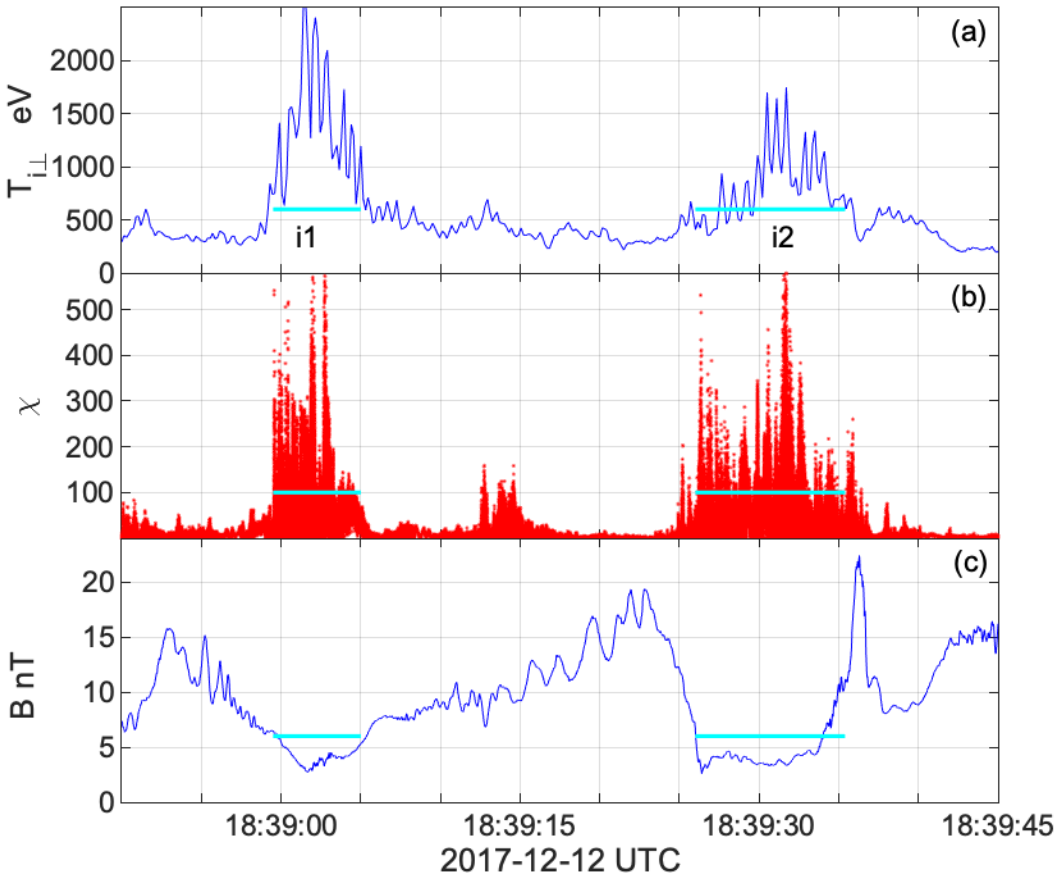

(a)
$T_{i\perp}$ eV
2000
1500
1000
500
0
i1
i2
(b)
χ
500
400
300
200
100
(c)
B nT
20
15
10
5
0
18:39:00
18:39:15
18:39:30
18:39:45
2017-12-12 UTC